Behavioural Brain Research 271 (2014) 258–268

Contents lists available at ScienceDirect

Behavioural Brain Research

journal homepage: www.elsevier.com/locate/bbr

Research report

REM sleep diversity following the pedunculopontine tegmental nucleus lesion in rat

Jelena Petrovic[a], Katarina Lazic[a], Aleksandar Kalauzi[b], Jasna Saponjic[a,*]

[a] University of Belgrade, Department of Neurobiology, Institute for Biological Research – Sinisa Stankovic, 11 060 Belgrade, Serbia
[b] University of Belgrade, Department for Life Sciences, Institute for Multidisciplinary Research, 11 030 Belgrade, Serbia

HIGHLIGHTS

- Pedunculopontine tegmental nucleus (PPT) is a source of thalamo-cortical innervation.
- PPT cholinergic neuronal loss potentiated the emergence of two REM sleep states.
- Pathological REM1 and REM2 have differential total EMG power.
- REM1 and REM2 have topographically distinct EEG microstructures.
- REM1 and REM2 have distinct cortical drive to dorsal nuchal musculature.

ARTICLE INFO

Article history:
Received 22 April 2014
Received in revised form 9 June 2014
Accepted 10 June 2014
Available online 17 June 2014

Keywords:
REM sleep
The pedunculopontine tegmental nucleus
Excitotoxic lesion
EEG
EMG
Cortico-muscular coherence

ABSTRACT

The aim of this study was to demonstrate that two REM clusters, which emerge following bilateral pedunculopontine tegmental nucleus (PPT) lesions in rats, are two functionally distinct REM states.

We performed the experiments in Wistar rats, chronically instrumented for sleep recording. Bilateral PPT lesions were produced by the microinfusion of 100 nl of 0.1 M ibotenic acid (IBO). Following a recovery period of 2 weeks, we recorded their sleep for 6 h. Bilateral PPT lesions were identified by NADPH – diaphorase histochemistry.

We applied Fourier analysis to the signals acquired throughout the 6 h recordings, and each 10 s epoch was differentiated as a Wake, NREM or REM state. We analyzed the topography of the sleep/wake states architecture and their transition structure, their all state-related EEG microstructures, and the sensorimotor (SMCx) and motor (MCx) cortex REM related cortico-muscular coherences (CMCs).

Bilateral PPT lesion in rats increased the likelihood of the emergence of two distinct REM sleep states, specifically expressed within the MCx: REM1 and REM2. Bilateral PPT lesion did not change the sleep/wake states architecture of the SMCx, but pathologically increased the duration of REM1 within the MCx, alongside increasing Wake/REM1/Wake and NREM/REM2/NREM transitions within both cortices. In addition, the augmented total REM SMCx EEG beta amplitude and REM1 MCx EEG theta amplitude was the underlying EEG microstructure pathology.

PPT lesion induced REM1 and REM2 are differential states with regard to total EMG power, topographically distinct EEG microstructures, and locomotor drives to nuchal musculature.

1. Introduction

REM sleep behavioral disorder (RBD) is a unique parasomnia characterized by the loss of normal skeletal muscle atonia and dream enactment behavior during REM sleep. Although RBD can be triggered pharmacologically [1], it is generally related to structural lesions within the midbrain and pontomedullary brainstem, with consequent uninhibited control of the motor cortex relating to limbs, most likely bypassing basal ganglia or other modulatory structures [1–4]. In humans RBD can be associated with pontomedullary strokes [2], narcolepsy, limbic encephalitis, Gullain-Barre syndrome, pharmacological agents (tricyclic or serotonergic antidepressants, alcohol, and beta blockers), and with a range of neurodegenerative diseases, including progressive supranuclear palsy, corticobasal syndrome, frontotemporal

* Corresponding author at: University of Belgrade, Department of Neurobiology, Institute for Biological Research – Sinisa Stankovic, Despot Stefan Blvd., 142, 11060 Belgrade, Serbia. Tel.: +381 11 2078426; fax: +381 11 2761433.
E-mail addresses: jasnasaponjic@yahoo.com, jasnasap@ibiss.bg.ac.rs (J. Saponjic).

http://dx.doi.org/10.1016/j.bbr.2014.06.026
0166-4328/

dementia and Huntington's disease [1]. Additionally, idiopathic RBD is most often caused by one of the synuclein-mediated neurodegenerative diseases [Parkinson's disease (PD), Lewy body dementia (LBD), and multiple system atrophy (MSA)], so that more than 80% of patients with RBD eventually develop PD, LBD or MSA [5].

RBD is the strongest clinical predictor for the onset of the neurodegenerative diseases [2,6], and presents a unique opportunity to study the progression of these neurodegenerative diseases and to develop neuroprotective therapies aimed at the prevention of the PD, MSA and LBD [7,8].

The pedunculopontine tegmental nucleus (PPT), being the main brain source of the thalamo-cortical cholinergic innervation, is postulated to have important functions relevant to the regulation of REM [9], arousal [10], and various motor control systems [11], including breathing control [12–15]. PPT is also postulated as the high relay nucleus for overall REM sleep phenomenon control, and each REM sleep event, executed by distinct cell groups within the brainstem, may be triggered and modulated by the activation of the PPT [10]. Anatomical studies support the theory that the PPT plays a key role in controlling the REM sleep phenomenon: each individual REM-sleep-sign generating nucleus receives afferent inputs from the PPT [16,17]. Additionally, direct projections from the PPT reach both the basal forebrain and the thalamus [18], and therefore the PPT operates as the control relay nucleus for the integrated contributions of these two cholinergic systems to the regulation of cortical activation [19,20].

PPT may be severely affected by PD pathology, and is regarded as a promising target for therapeutic deep-brain stimulation [21]. Although PD is a neurodegenerative disease, whose cardinal manifestations are due primarily to dopaminergic dysfunction within the brain, PD may also involve the loss of PPT cholinergic neurons [22,23], and the degeneration of about 50% of the PPT cholinergic neurons in PD has been reported [24]. Cortical and thalamic subcortical cholinergic denervations, due to the degeneration of PPT cholinergic neurons, have also been related to RBD [22], as well as to gait and balance impairment, including falls in PD [24,25].

However, our understanding of the PPT role in PD pathogenesis is limited by the lack of a suitable model of PPT cholinergic neuronal degeneration. So far, the animal models used to investigate the pathogenesis and pathophysiology of PD have mostly been based on the systemic or local administration of neurotoxins selective for dopaminergic neurons of the substantia nigra (such as MPTP, 6-OHDA, LPS, proteosome inhibitors, rotenone, and paraquat), but there have also been pharmacological and transgenic models in mice and rats [26–29]. Both toxic and transgenic animal models have their own specificities and limitations, and the certain toxin selectivity or interspecies anatomical and morphological brain structure differences must be carefully taken into consideration when choosing the model to be used and when interpreting the results. For example, recent studies using different toxins (6-OHDA vs. Lactacystin) for local injection into the substantia nigra for the destruction of the dopaminergic nigro-striatal pathway [21,30] demonstrated different results within the PPT, as a consequence of substantia nigra dopaminergic neuronal loss: mostly non-cholinergic PPT neuronal loss [30] versus mostly PPT cholinergic loss [21]. These studies suggest the Lactaystin PD rat model as a more suitable model for investigating the role of the PPT in PD.

Our recent studies on the rat models of functionally distinct cholinergic neuropathology showed evidence that only broad cortical cholinergic neuronal innervation loss induced transient, and topographically specific, sleep/wake states disturbance, as well as Wake and REM theta augmentation over 3 weeks [31,32]. Indeed even mild sustained thalamo-cortical cholinergic neuronal innervation loss (across 5 weeks) disturbs the sleep/wake states transition structure and the sleep/wake states related "EEG microstructure", expressed as augmented cortical activation during all sleep/wake states [33], alongside the two clusters of REM which emerged (REM1 – REM without atonia, and REM2 – REM with atonia).

Since both the basic and clinical studies suggest that RBD pathogenesis stems from a breakdown in the brainstem circuits controlling REM sleep atonia [2,8], and that PPT acts as the central relay nucleus for the overall REM sleep phenomenon, including REM atonia control [10], we assume that the two REM clusters, emerging in our rat model of the bilateral PPT lesion [31,33], represent two distinct REM states. Therefore, this study is aimed to prove that the two REM clusters, which emerge following bilateral PPT lesions in rats, are two functionally distinct REM states.

2. Materials and methods

We performed the experiments in 33 adult male Wistar rats, chronically instrumented for sleep recording, and assigned to two experimental groups: physiological controls ($n = 16$) and bilaterally PPT lesioned rats ($n = 17$). Prior to surgery and consistently throughout the experimental protocol, the animals were maintained on a 12 h light–dark cycle, and were housed at 25 °C with free access to food and water.

All animal procedures were in compliance with the EEC Directive (86/609/EEC) on the protection of animals used for experimental and other scientific purposes, and were approved by the Ethical Committee for the Use of Laboratory Animals of the Institute for Biological Research "Sinisa Stankovic", University of Belgrade (Approval No. 2-21/10).

2.1. Surgical procedure

The surgical procedures employed for the chronic electrode implantation for sleep recording have been described previously [34], and are outlined below. We implanted two epidural parietal stainless-steel screw electrodes for EEG cortical activity recording from the motor (A/P: +1.0; R/L: 2), and the sensorimotor (A/P: −3.0; R/L: 2) cortex under ketamine/diazepam anesthesia (Zoletil 50, VIRBAC, France, 50 mg/kg; i.p.) [31–33,35]. Bilateral electromyogram (EMG) wire electrodes were implanted into the dorsal nuchal musculature to assess skeletal muscle activity. A referential stainless-steel screw electrode was implanted in the nasal bone. All the electrode leads were soldered to a miniature connector plug (39F1401, Newark Electronics, Schaumburg, IL, USA), and the assembly was fixed to the screw electrodes and skull using acrylic dental cement (Biocryl-RN, Galenika a.d. Beograd, Serbia).

During the operation procedure for the chronic electrodes implantation we performed the bilateral PPT lesions by the stereotaxically guided microinfusion of 0.1 M ibotenic acid (IBO)/0.1 M PBS into the right and left PPT (A/P: −7.8; R/L: 1.9; D/V: 7 from the brain surface), using a Digital Lab Standard Stereotaxic Instrument with a Quintessential Stereotaxic Injector (Stoelting Co., Wood Dale, IL, USA), and a Hamilton syringe (1 μl). The IBO concentration (Sigma; pH = 7.4) was chosen based on previous studies [31,33,36].

The microinfusions were done in a volume of 100 nl, using a single, 60 s pulse. Following the first microinfusion, a Hamilton syringe was left within the local brain tissue for 5 min, before its removal from the brain, allowing the solution to diffuse within the PPT, and then washed out with saline before the next microinfusion within the contralateral PPT.

2.2. Recording procedure

At the end of the surgical procedure, the scalp wounds were sutured and the rats were allowed to recover for 2 weeks before their adaptation to the recording cable and plexiglass chamber

(30 cm × 30 cm × 30 cm) for one day. The EEG and EMG activities were carried from the connector plug on the rat head by the cable, and passed through a sealed port on the recording box. The activities were displayed on a computer monitor, and stored on disk for further off-line analysis.

After conventional amplification and filtering (0.3–100 Hz band pass; A-M System Inc. Model 3600, Carlborg, WA, USA), the analog data were digitized (sampling frequency 256 s^{-1}), and recorded for 6 h, during the normal inactive circadian phase for rats (from 9 a.m. to 3 p.m.), using DataWave SciWorks Experimenter Verson 8.0 (Datawave Technologies, Longmont, CO, USA).

2.3. Tissue processing and histochemistry

At the end of the recording sessions the PPT lesion was identified using NADPH – diaphorase histochemistry [37]. The rats were deeply anesthetized and perfused transcardially, starting with a vascular rinse until the liver had been cleared (200 ml of 0.9% saline; perfusion speed of 40 ml/min); followed by a 4% paraformaldehyde solution in 0.1 M PBS (200 ml; 100 ml at 40 ml/min, and then 30 ml/min), and finally with a 10% sucrose solution in 0.1 M PBS (200 ml; 30 ml/min). The animals were sacrificed and the brains were extracted, cleared of the meninges and blood vessels, and immersed in 4% paraformaldehyde overnight, and then in a 30% sucrose solution for several days. The brains were cut along a transverse plane into 40 μm-thick sections using a cryotome, and the free-floating sections were stained, mounted, and coverslipped with DPX (Sigma), and examined under a Zeiss Axiovert microscope equipped with a camera. We quantified the PPT cholinergic cell loss using Image J 1.46 software. NADPH – diaphorase positive cells were counted in three 40 μm thick coronal sections per brain within the overall rostro-caudal PPT dimension [31–33].

2.4. Data analysis

We included in the data analysis the signals recorded from the control rats and all the rats with positively identified bilateral PPT lesions. A typical example of a histologically identified and quantified bilateral PPT lesion throughout the overall PPT rostro-caudal dimension is depicted in Fig. 1.

Analysis of the recorded signals was conducted using software we developed using MATLAB 6.5. We applied Fourier analysis to the signals acquired throughout each 6 h recording (2160 10 s Fourier epochs), and each 10 s epoch was differentiated as Wake, NREM or REM state for further analysis of the Wake, NREM and REM related EEG amplitudes of all the conventional frequency bands (δ = 0.3–4 Hz; θ = 4.1–8 Hz; σ = 10.1–15 Hz; β = 15.1–30 Hz; γ = 30.1–50 Hz) of the control and bilaterally PPT lesioned rats. First, we extracted all the 10 s Wake epochs from each 6 h recording, based on the product of EEG sigma and theta frequency power on the *y*-axis, and the total EMG power on the *x*-axis. Further, the differentiation of NREM and REM 10 s epochs was done using the total EMG power on the *y*-axis, and the EEG delta/theta power ratio on the *x*-axis. The typical scattergrams of the sleep/wake states differentiation using EEG recorded from the sensorimotor (SMCx) and the motor (MCx) cortex of the control and PPT lesioned rat are depicted in Fig. 2.

In this study we particularly analyzed two distinct REM clusters differentiated within the scattergrams of the bilaterally PPT lesioned rats. For the REM clusters analysis, each REM epoch was differentiated, based on the EMG power and two-cluster *K*-means algorithm, as either REM without atonia (REM1), or REM with atonia (REM2). For the total REM/REM1/REM2 EEG amplitude changes, we calculated group probability density distributions for all the relative amplitudes of the conventional EEG frequency bands per 6 h, using the probability density estimate (PDE) routine supplied with MATLAB 6.5 [31–33]. For each REM (total REM, REM1, REM2), and each frequency band, PDE analysis was performed on the ensembles of relative amplitudes by pooling measured values from all the animals belonging to the specific group (control or bilateral PPT lesion).

For all experimental groups we also analyzed the mean number of all the transition states during the 6 h of the sleep recordings (Wake/NREM, NREM/Wake; Wake/REM, REM/Wake; Wake/REM1, REM1/Wake; Wake/REM2, REM2/Wake; NREM/REM, REM/NREM; NREM/REM1, REM1/NREM; NREM/REM2, REM2/NREM). For the transition state analysis, the sleep/wake states (Wake, NREM, REM, REM1, REM2) were determined for each 5 s epoch [31,33,38].

In order to further functional REM clusters differentiation we also analyzed the total REM/REM1/REM2 cortico-muscular coherences (CMCs) separately, for all the conventional EEG frequency bands, between the SMCx or MCx, and the EMG of the dorsal nuchal muscles.

CMC values were calculated using the "cohere" routine of the MATLAB 6.5 Signal Processing Toolbox. It actually computes the magnitude squared coherence between signals *x*(EEG) and *y*(EMG) as

$$C_{xy}(f) = \frac{|P_{xy}(f)|^2}{P_{xx}(f)P_{yy}(f)}$$

where $P_{xy}(f)$ stands for the cross spectrum of *x* and *y*, while $P_{xx}(f)$ and $P_{yy}(f)$ denote the power spectra of the two signals.

All CMC values were determined for every 10 s of each 6 h recording, and the group means were calculated for each EEG conventional frequency band (δ, θ, σ, β, γ), each REM state (total REM/REM1/REM2), and each group of animals (control or bilateral PPT lesion).

For the statistical analysis of the PDE/6 h and CMC/6 h we calculated the relative amplitude means for Wake and NREM per each 60 min, and for the total REM, REM1, REM2 per each 30 min.

We employed the Mann–Whitney *U* two-tailed tests for the statistical analysis of all group means over 6 h: the group mean numbers of 10 s epochs of Wake, NREM, total REM, REM1, REM2; the group means of total REM/REM1/REM2 EEG relative amplitudes for all frequency bands; the group mean numbers of all transition states; and the group CMCs means of the total REM, REM1, and REM2.

3. Results

3.1. Sleep/wake state architecture and transition structure following the bilateral PPT lesion

The bilateral PPT lesion did not change the sleep/wake states architecture within SMCx 14 days after the lesion. The duration of the Wake/NREM/total REM/REM1/REM2 over 6 h in the SMCx was equal in controls versus lesioned rats ($z \geq -0.69$, $p \geq 0.52$). At the same time in the MCx, while Wake/NREM duration/6 h did not change ($z \geq -1.24$, $p \geq 0.24$), REM duration did increase ($z = -2.31$, $p = 0.02$), but only due to the increased duration of REM1 ($z = -2.62$, $p = 0.006$).

Sleep/wake states transition structure analysis has shown increased Wake to REM, and REM to Wake transitions in the SMCx and MCx ($z \geq -6.43$, $p \leq 0.001$), which is only due to the increased Wake to REM1 and REM1 to Wake transitions ($z \geq -4.25$, $p \leq 0.02$; Figs. 3A and 4A and Table 1). This pathological transition structure was expressed alongside the increased NREM to REM, and REM to NREM transitions within both cortices ($z \geq -4.24$, $p \leq 0.005$), and it is caused by increased NREM to REM2, and REM2 to NREM transitions ($z \geq -4.90$, $p \leq 10^{-4}$; Figs. 3B and 4B and Table 2).

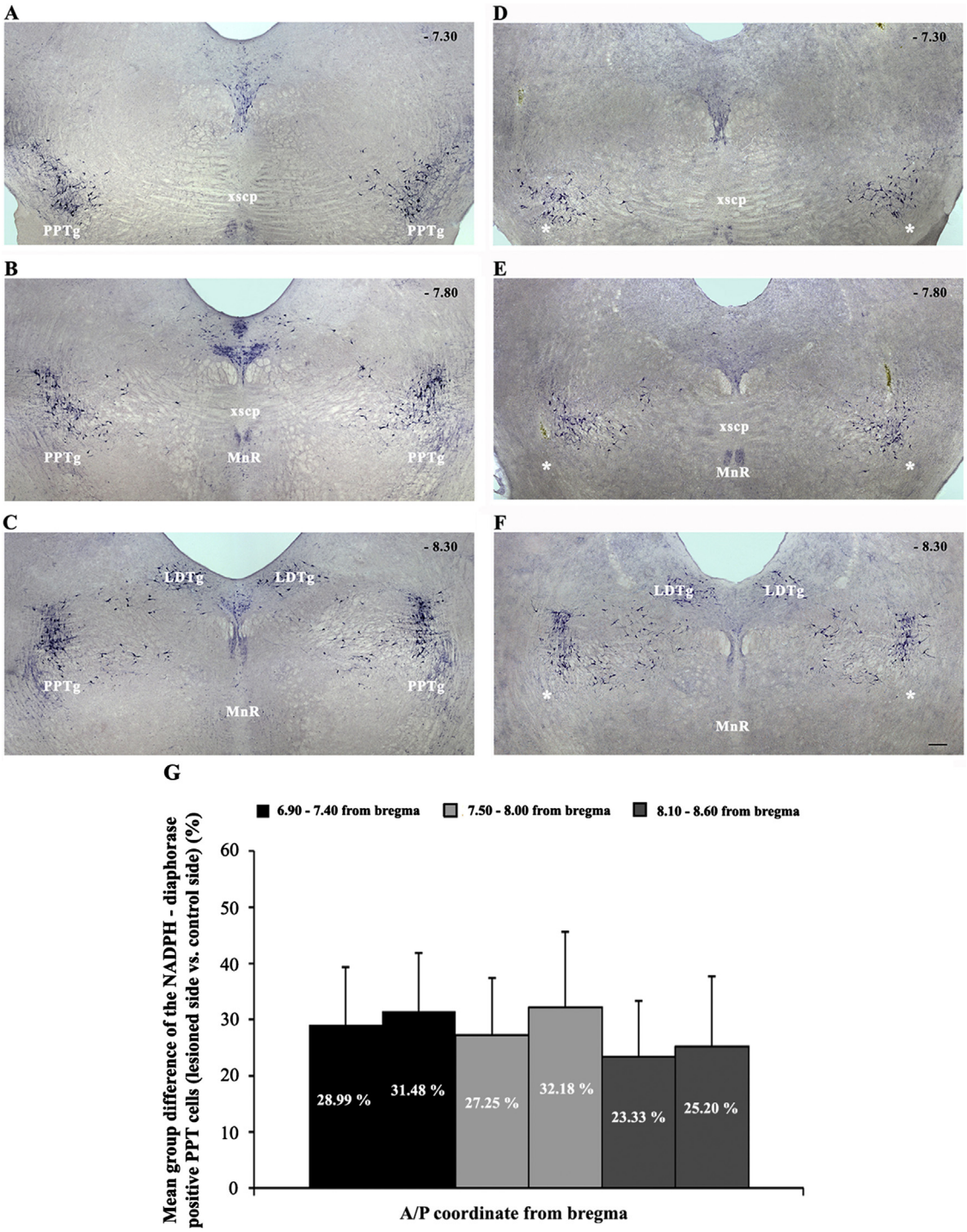

Fig. 1. Typical example of a histologically identified bilateral PPT lesion throughout the overall PPT rostro-caudal dimension (from −6.90–8.30 mm caudal to bregma): control PPT (A–C) versus bilateral PPT lesion (D–F), and the group data of cholinergic neuronal loss ($n = 17$), quantified throughout the overall rostro-caudal dimension of each PPT (G). The cholinergic neuronal loss, expressed as the mean group difference of NADPH – diaphorase positive cells, per each stereotaxic range, throughout each PPT rostro-caudal dimension, of PPT lesioned versus control brains ± SD in %. Although the cholinergic neuronal loss was >23.33 ± 10.03% throughout the overall rostro-caudal dimension of each PPT, the maximal cholinergic loss was >28.99 ± 10.35% from 6.90 to 7.40 caudal to bregma. PPTg – pedunculopontine tegmental nucleus; xscp – decussation of the superior cerebellar peduncle; MnR – median raphe nucleus; LDTg – laterodorsal tegmental nucleus. White stars mark the lesioned PPT. Scale bar is 200 μm.

3.2. Topography of the REM EEG microstructure caused by bilateral PPT lesion

The Bilateral PPT lesion augmented the EEG beta amplitude within the SMCx, expressed only during total REM ($z = -2.12$, $p = 0.03$; Fig. 5), alongside the simultaneously augmented EEG theta amplitude within the MCx ($z = -2.31$, $p = 0.02$; Fig. 6), only during REM1 (REM without atonia).

3.3. Diversity of the REM-related CMCs following bilateral PPT lesion

The REM1 and REM2-related SMCx/MCx EEG and EMG spectra of the controls and bilaterally PPT lesioned rats, which were used for the CMCs analysis, are shown in Fig. 7.

The impact of bilateral PPT lesions on the REM-related SMCx and MCx cortico-muscular coherences (CMCs) is depicted in Table 3.

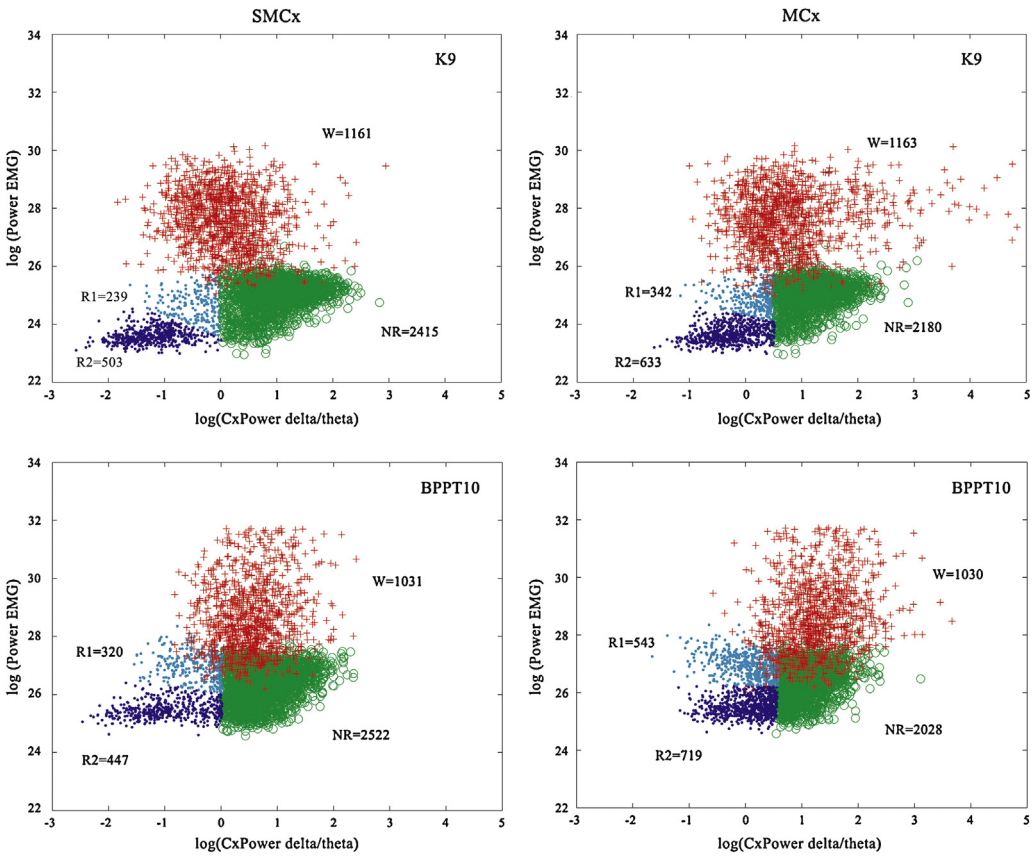

Fig. 2. Examples of the final scattergrams for Wake/NREM/REM differentiation within the sensorimotor (SMCx, left column) and motor cortex (MCx, right column) in the 6 h sleep recording of the control rat (K9), and the bilaterally PPT lesioned rat (BPPT10). In all scattergrams the Wake 10 s epochs (W cluster, crosses) are transferred to these final scattergrams from the preceding Wake/Sleep differentiations. NR cluster, circles – NREM 10 s epochs; R1, R2 clusters, dots – REM1, REM2 10 s epochs.

Table 1
Group mean number of Wake/REM/Wake transitions/6 h ± SEMs.

	Wake to REM	REM to Wake	Wake to REM1	REM1 to Wake	Wake to REM2	REM2 to Wake
SMCx						
Control	10.19 ± 0.91	11.60 ± 0.78	4.40 ± 0.45	5.20 ± 0.44	11.80 ± 1.28	11.10 ± 1.17
Lesion	**27.28 ± 2.16**	**26.62 ± 2.06**	**8.61 ± 0.91**	**9.50 ± 0.92**	12.73 ± 1.36	11.60 ± 1.00
MCx						
Control	16.37 ± 0.80	16.46 ± 0.77	5.29 ± 0.54	5.40 ± 0.40	11.38 ± 0.71	11.07 ± 0.62
Lesion	**22.48 ± 1.41**	**22.87 ± 1.43**	**8.47 ± 1.01**	**8.75 ± 0.80**	13.39 ± 0.63	11.02 ± 0.59

Bold numbers indicate the statistically significant mean values at $p \leq 0.02$.

Table 2
Group mean number of NREM/REM/NREM transitions/6 h ± SEMs.

	NREM to REM	REM to NREM	NREM to REM1	REM1 to NREM	NREM to REM2	REM2 to NREM
SMCx						
Control	46.46 ± 2.44	46.44 ± 2.51	25.15 ± 1.59	22.75 ± 1.65	14.58 ± 1.21	16.56 ± 1.32
Lesion	**60.58 ± 3.68**	**61.10 ± 3.77**	26.76 ± 1.48	24.63 ± 1.57	**29.69 ± 2.25**	**31.44 ± 2.45**
MCx						
Control	73.96 ± 3.22	74.24 ± 3.19	48.97 ± 2.39	48.77 ± 2.50	29.26 ± 1.71	30.00 ± 1.62
Lesion	**93.46 ± 2.58**	**92.81 ± 2.54**	55.11 ± 2.72	53.81 ± 2.62	**41.58 ± 2.06**	**41.99 ± 1.89**

Bold numbers indicate the statistically significant mean values at $p \leq 0.005$.

Our results show the highest control SMCx and MCx CMCs values of theta and sigma during total REM. In contrast to the highest control sigma REM1-related CMCs values (REM without atonia, Fig. 2 and Table 3), the highest control theta CMCs expression was during REM2 (REM with atonia, Fig. 2 and Table 3).

The bilateral PPT lesion decreased the total REM sigma CMCs ($z \geq -2.97$, $p \leq 0.005$) due to both REM2-related sigma SMCx and MCx CMCs decreases ($z \geq -3.98$, $p \leq 0.001$; Table 3). While the MCx REM2-related sigma CMC decrease occurred alongside the theta CMC decrease ($z = -2.91$, $p = 0.002$; Table 3), the SMCx REM2-related sigma CMC decreased together with the theta, beta and gamma CMCs decreases ($z \geq -3.60$, $p \leq 0.01$; Table 3).

While the bilateral PPT lesion severely, and dominantly, altered REM2-related CMCs, it only induced REM1-related SMCx CMC beta decrease ($z = -2.07$, $p = 0.04$; Table 3).

In our rat model of the thalamo-cortical cholinergic denervation, the REM2-related CMCs disturbances, through the impact of the SMCx drive to dorsal nuchal muscles, were dominant.

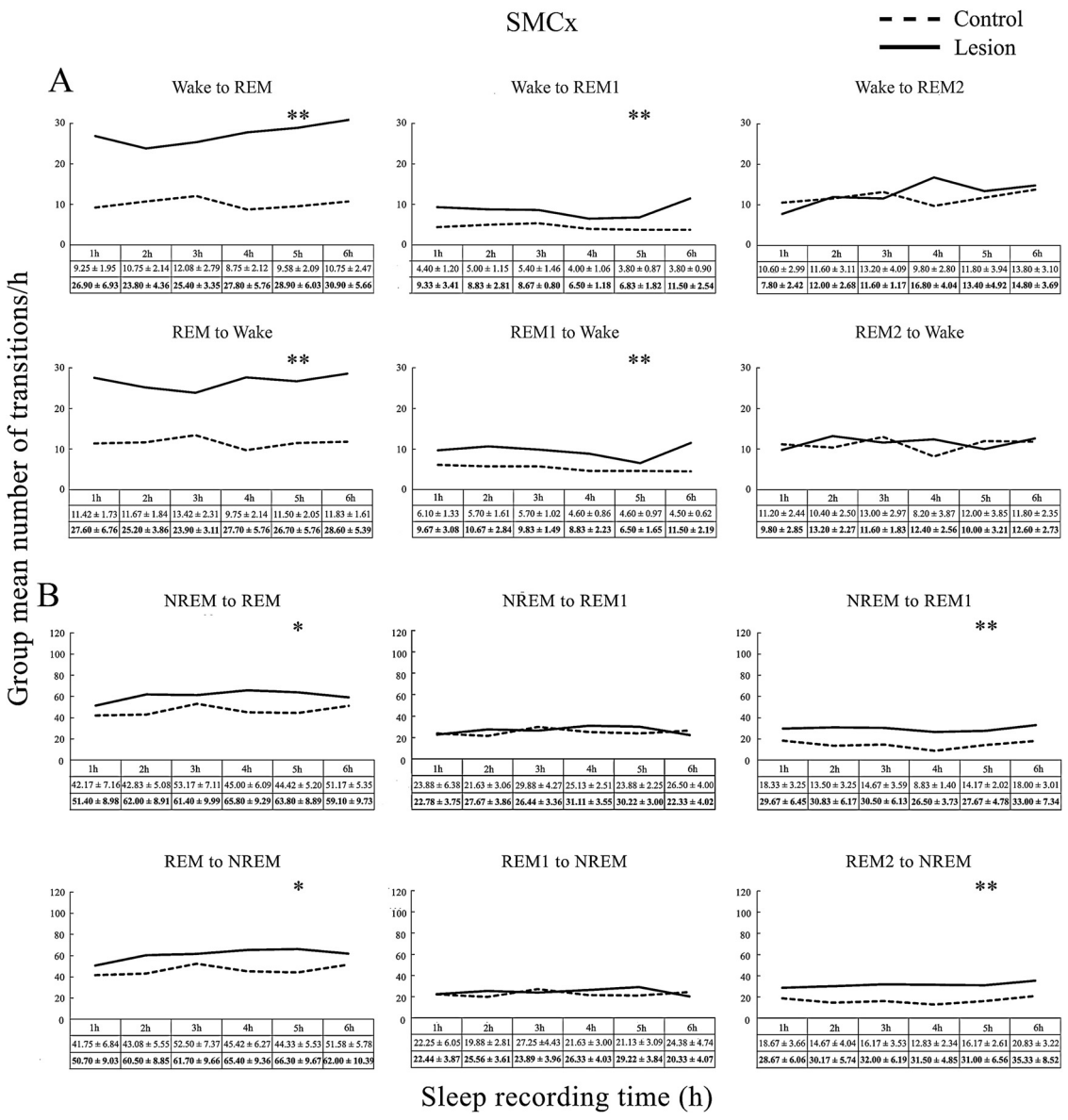

Fig. 3. Line diagrams of the group mean numbers for all Wake/REM/Wake (A) and NREM/REM/NREM (B) transitions per 1 h ± SEMs, 14 days after the bilateral PPT lesions (Lesion, solid line) versus the control group (Control, dashed line) within the sensorimotor cortex (SMCx). $^{**}p \leq 10^{-4}$; $^{*}p \leq 0.02$.

These disturbances were expressed as the impairment of the total REM/REM1/REM2-related beta CMCs ($z \geq -4.31$, $p \leq 0.04$; Table 3).

4. Discussion

Our study demonstrates for the first time that the bilateral PPT lesion in rats can give rise to the emergence of two distinct REM sleep states, particularly expressed within the MCx: REM1 (REM without atonia, or "sigma coherent REM"), and REM2 (REM with atonia, or "theta coherent REM"). We have shown that 14 days following the bilateral PPT lesion the total REM duration increased only in MCx, due to the increased REM1 duration, while there were pathologically enhanced Wake to REM1 and REM1 to Wake transitions (Figs. 3A and 4A and Table 1), alongside the simultaneously enhanced NREM to REM2, and REM2 to NREM transitions (Figs. 3B and 4B and Table 2) in the both cortices (SMCx and MCx). Additionally, the REM sleep EEG microstructures showed significant augmentation of the total REM EEG beta amplitude within the SMCx (Fig. 5), alongside significantly augmented REM1 EEG theta amplitude within the MCx (Fig. 6).

Aside from the differential total EMG power of the dorsal nuchal musculature (Fig. 2), REM1 and REM2 have topographically distinct EEG microstructures (Figs. 5 and 6) and cortical locomotor drive to dorsal nuchal musculature (Table 3). On the basis of the CMC values, we have shown that the dominant impact of the bilateral PPT lesion occurred during the REM2 state, while the REM1 state was stable, except for an impaired beta related CMC, as a consequence of the altered locomotor drive from the SMCx caused by the PPT lesion.

Our recent studies demonstrate that bilateral PPT cholinergic thalamo-cortical control impairment sustainably disturbs the sleep/wake state transition structure and augments cortical activation during all sleep/wake states. These changes are expressed as the long-lasting augmentation of the EEG beta and gamma amplitudes and the attenuation of the EEG delta amplitudes during Wake and NREM sleep [31,33]. These pathological sleep/wake states related EEG microstructures and transition structures were topographically specific, and particularly noted within the MCx [31]. These studies investigated the sleep/wake states architecture of three main brain states, and their transition structure, alongside their underlying EEG microstructure, and demonstrated that the

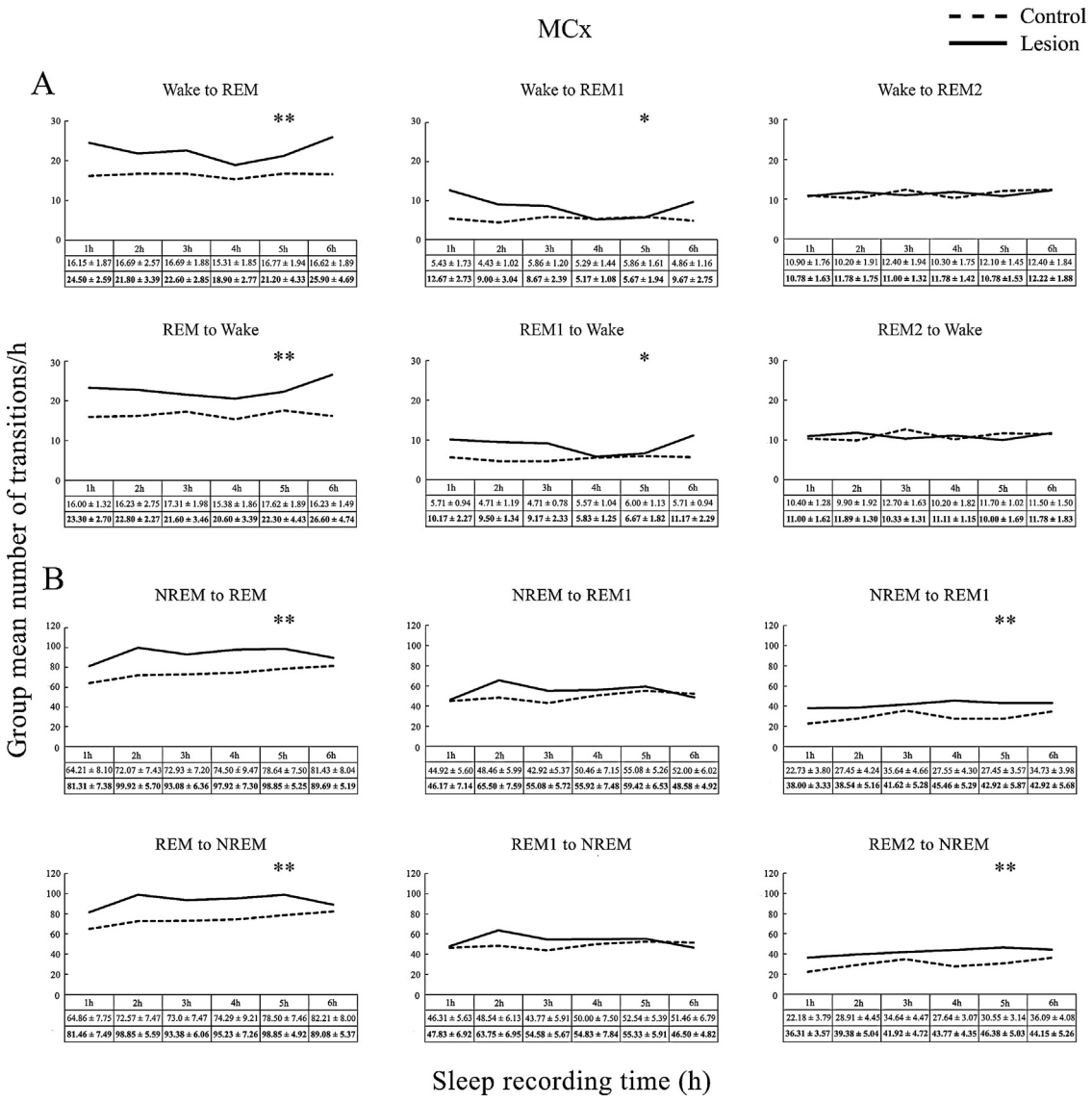

Fig. 4. Line diagrams of the group mean numbers for all Wake/REM/Wake (A) and NREM/REM/NREM (B) transitions per 1 h ± SEMs, 14 days after the bilateral PPT lesions (Lesion, solid line) versus the control group (Control, dashed line) within the motor cortex (MCx). $^{**}p \leq 10^{-4}$; $^{*}p \leq 0.02$.

Table 3
Group means of REM-related cortico-muscular coherences (CMCs)/6 h ± SEMs.

	Delta	Theta	Sigma	Beta	Gamma
SMCx CMC					
REM					
Control	0.10 ± 0.01	0.12 ± 0.01	0.12 ± 0.01	0.09 ± 0.01	0.08 ± 0.01
Lesion	0.08 ± 0.01	0.11 ± 0.01	**0.08 ± 0.01**	**0.04 ± 0.00**	**0.04 ± 0.01**
REM1					
Control	0.09 ± 0.01	0.08 ± 0.01	0.15 ± 0.02	0.09 ± 0.01	0.05 ± 0.01
Lesion	0.07 ± 0.01	0.06 ± 0.01	0.10 ± 0.02	**0.05 ± 0.01**	0.04 ± 0.01
REM2					
Control	0.09 ± 0.01	0.23 ± 0.01	0.09 ± 0.00	0.08 ± 0.01	0.09 ± 0.01
Lesion	0.07 ± 0.01	0.16 ± 0.02	**0.04 ± 0.01**	**0.03 ± 0.00**	**0.04 ± 0.01**
MCx CMC					
REM					
Control	0.09 ± 0.01	0.12 ± 0.01	0.12 ± 0.01	0.06 ± 0.00	0.03 ± 0.00
Lesion	0.12 ± 0.01	0.13 ± 0.01	**0.09 ± 0.01**	0.06 ± 0.01	0.03 ± 0.00
REM1					
Control	0.08 ± 0.00	0.06 ± 0.01	0.11 ± 0.01	0.06 ± 0.01	0.02 ± 0.00
Lesion	0.08 ± 0.01	0.06 ± 0.01	0.13 ± 0.01	0.07 ± 0.00	0.03 ± 0.00
REM2					
Control	0.06 ± 0.00	0.21 ± 0.02	0.10 ± 0.01	0.06 ± 0.00	0.03 ± 0.00
Lesion	0.06 ± 0.01	**0.12 ± 0.02**	**0.04 ± 0.01**	0.05 ± 0.01	0.03 ± 0.00

Bold numbers indicate the statistically significant mean values at $p \leq 0.04$.

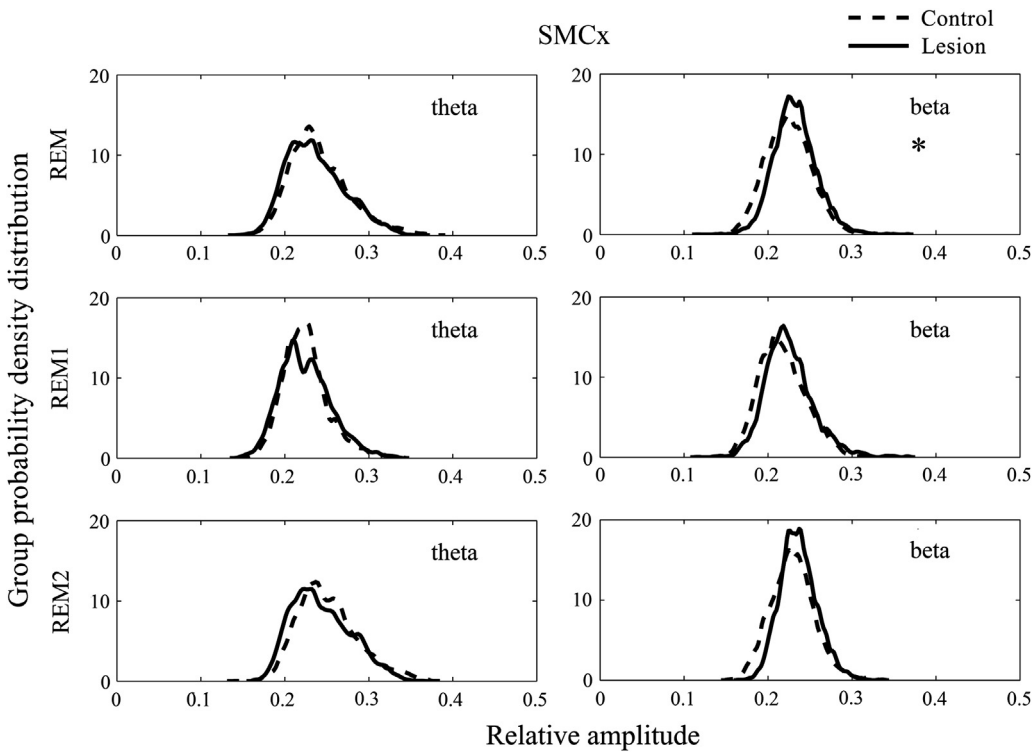

Fig. 5. REM/REM1/REM2 EEG microstructures 14 days after the bilateral PPT lesion: the group probability density distributions of total REM/REM1/REM2 theta (left column), and total REM/REM1/REM2 beta (right column) relative amplitudes within the sensorimotor cortex (SMCx). Lesion – solid line; Control – dashed line; $^{*}p = 0.03$.

PPT cholinergic neuronal loss approximately > 20% throughout the overall rostro-caudal PPT dimension for each PPT [33].

Our present study includes two types of REM (REM1 and REM2) in the sleep/wake states analysis that emerged within the scattergrams of sleep/wake states differentiation following the bilateral PPT lesion, particularly within the MCx scattergrams. REM1 10 s epochs from the scattergram show REM epochs with a higher total dorsal nuchal muscles EMG power (REM without atonia) while the REM2 10 s epochs show REM epochs with a lower total dorsal nuchal muscles EMG power (REM with atonia). CMCs analysis enabled us to demonstrate that the total REM state of the control group is the state with the highest sigma and theta coherence:

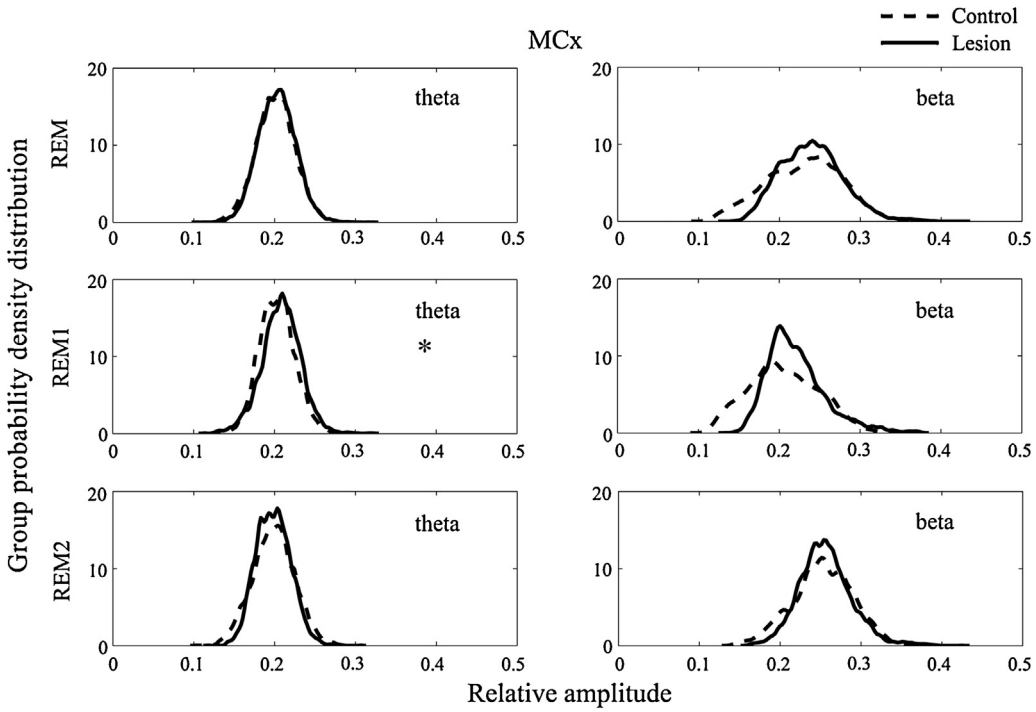

Fig. 6. REM/REM1/REM2 EEG microstructures 14 days after the bilateral PPT lesion: the group probability density distributions of total REM/REM1/REM2 theta (left column), and REM/REM1/REM2 beta (right column) relative amplitudes within the motor cortex (MCx). Lesion – solid line; Control – dashed line; $^{*}p = 0.02$.

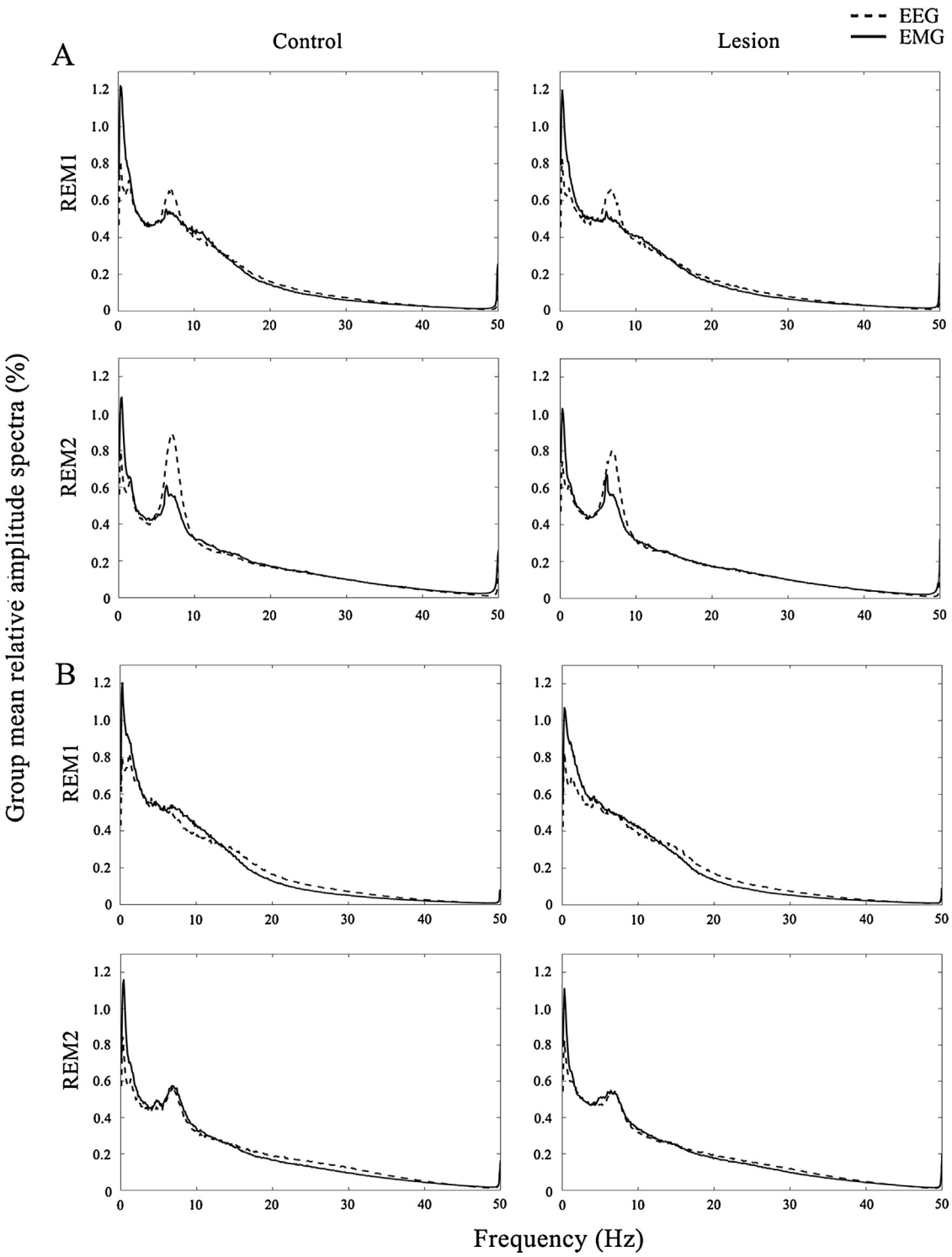

Fig. 7. REM1 and REM2 group mean relative amplitude spectra of the SMCx (A) and MCx (B) EEG (dashed line), and the dorsal nuchal muscles EMG (solid line) of the control rats (Control) and bilaterally PPT lesioned rats (Lesion), used for the cortico-muscular coherence (CMC) analysis of all conventional frequency bands.

whereas control group REM1 is the state with the highest sigma coherence, control group REM2 is the state with the highest theta coherence. The bilateral PPT lesion severely altered REM2-related CMCs (the impaired sigma CMCs is followed by impaired theta, beta and gamma CMCs), while there was only REM1-related SMCx beta CMC impairment, induced through the altered SMCx – nuchal muscles drive.

There is evidence that the oscillatory activity of the SMCx shows coherence in the beta frequency range with the EMG during weak to moderately steady contractions in both animals and humans. This beta CMC is regarded as an efferent phenomenon, or an oscillation that is propagated from the cortical source to the spinal motoneurons via the corticospinal tract [39,40]. CMC quantitatively reflects the corticomotoneuronal coupling, which can be used as an index of

the cortical locomotor drive to particular motor output [39]; represents a binding mechanism between the motor cortex and the corresponding muscle; reflects the conduction of fast pyramidal pathways, and plays a crucial role in sensorimotor integration [41]. CMC is an established method for quantifying the functional coupling between the motor cortex and the contralateral peripheral muscle in the frequency domain and the measure of the integrity of the pyramidal system [42]. CMC is prominent in the beta frequency band during weak to medium isometric muscle contraction [43]. In contrast to tremor, which has been related to increased oscillatory beta band synchronization [42], the movement slowing (bradykinesia, akinesia, and rigidity) in PD has been related to decreased beta band CMC [44].

In a normal human brain, the beta band oscillatory activity is associated with the retention of ongoing motor activities. Although the pathology of PD is complex and involves multi-stage neuronal death throughout different parts of the brain [45], including pontine cholinergic neurons [22,23], enhanced beta oscillatory activity in PD is displayed across the cortico-basal ganglia pathway as one of the most prominent neurophysiological phenomena associated with the disorder [46]. Beta band oscillations are associated with both cognitive and motor functions in normal animals and humans, and are hypothesized to play a key role in the maintenance of the current behavioral state, or the maintenance of the status quo [47]. In this context the enhanced cortical beta amplitude during PD constantly signals to the rest of the brain to maintain the current state and reduce the number of shifts to different behaviors resulting in akinesia and bradykinesia [46]. It is well known that the output of the basal ganglia (the efferents from globus palidus internus and substantia nigra pars reticulata) is sent primarily to the thalamus and from there to the frontal cortex, forming the partially closed cortico-basal ganglia loop.

PPT as the main source of thalamo-cortical cholinergic innervation, and as a part of the ascending reticular activating system, monosynaptically innervates the substantia nigra and to less extent the globus palidus internus [48]. However, through its descending cholinergic efferents, PPT also indirectly, through REM sleep circuitry, promotes REM sleep atonia [8,49,50], and the degeneration of PPT cholinergic neurons could underlie the motor symptoms in patients with PD and RBD [8].

PPT is a heterogeneous structure, formed by an ensemble of cholinergic and non-cholinergic neurons split into two parts: a more cell-dense dorsolateral, caudal half of the nucleus – the pars compacta, and a more diffuse rostro-medial part – the pars dissipata. Cholinergic neurons account to only 50% of all neurons contained within the PPT, while approximately 40% of all PPT neurons are located within the PPT pars compacta. Although cholinergic neurons make up approximately 90% of the neuronal population within the PPT – the pars compacta, the cholinergic neurons compose 25–50% of the neuronal population within the PPT – the pars dissipata [16,51,52]. Although the anatomical and morphological PPT structure is similar in rodents, cats, non-human primates and humans, there are interspecies differences in architecture and the circuitry distribution of the cholinergic, glutamatergic or GABAergic neurons, as well as in the distribution of PPT afferent and efferent projections [52]. There is also evidence which demonstrates that the subpopulations of the PPT cholinergic neurons co-express glutamate, GABA, nitric oxide and Substance P [51]. In this study we did not follow the impact of PPT cholinergic neuronal loss, caused by the degeneration of dopaminergic neurons of substantia nigra, but we studied the impact of impaired PPT cholinergic control on sleep/wake states, particularly on the REM state. In our study, by using our microinfusion methodological approach, we induced incomplete, but selective bilateral PPT lesions within the limits of the PPT pars compacta, as a mainly cholinergic neuronal population of the PPT. But, since the PPT is a neurochemically heterogeneous structure, containing also the significant populations of GABAergic and glutamatergic neurons [53–56] and since we used ibotenic acid, as the mostly used and effective excitotoxin for non-selective lesions of neuronal cell bodies [36,57], we could not exclude the lesions of non-cholinergic neurons, and consequently their impact, at least to some degree. However, here in this study, we have demonstrated PPT cholinergic neuronal loss of approximately > 23% throughout the overall rostro-caudal PPT dimension for each PPT (Fig. 1G).

5. Conclusions

Our study demonstrates the emergence of two REM sleep states in the bilateral PPT lesion rat model for the first time, as well as the commonly impaired REM/REM1/REM2-related beta CMCs through the dominantly altered SMCx-dorsal nuchal muscles drive. Regarding the cortico-muscular coherences, the bilateral PPT lesion altered both REM1 and REM2 cortico-muscular control, but more severely during REM2. During REM2, the impaired beta CMC was additionally followed by the impaired theta, sigma and gamma CMCs, due to the altered SMCx-dorsal nuchal muscles drive, while the altered MCx-dorsal nuchal muscles drive is expressed as the impaired theta and sigma CMCs.

REM1 and REM2 are differential states with regard to the total EMG power, the topographically distinct EEG microstructures, and the SMCx and MCx locomotor drive to the dorsal nuchal musculature.

Our results indicate the simultaneous breakdown of the PPT cholinergic direct ascending thalamo-cortical control, and the indirect descending control of the REM sleep atonia regulatory circuitry, for the emergence of two differential REM states following bilateral PPT lesion in rats.

Acknowledgement

This work was supported by a Serbian Ministry of Education, Science and Technological Development Grant OI 173022.

References

[1] Postuma RB, Gagnon JF, Montplaisir JY. REM sleep behavior disorder: from dreams to neurodegeneration. Neurobiol Dis 2012;46:553–8.
[2] Boeve BF, Silber MH, Saper CB, Ferman TJ, Dickson DW, Parisi JE, et al. Pathophysiology of REM sleep behaviour disorder and relevance to neurodegenerative disease. Brain 2007;30:2770–88.
[3] Luppi PH, Clement O, Sapin E, Gervasoni D, Peyron C, Leger L, et al. The neuronal network responsible for paradoxical sleep and its dysfunctions causing narcolepsy and rapid eye movement (REM) behavior disorder. Sleep Med Rev 2011;15:153–63.
[4] Sapin E, Lapray D, Berod A, Goutagny R, Leger L, Ravassard P, et al. Localization of the brainstem GABAergic neurons controlling paradoxical (REM) sleep. PLoS ONE 2009;4:e4272.
[5] Boeve BF. Idiopathic REM sleep behavior disorder in the development of Parkinson's disease. Lancet Neurol 2013;12:469–82.
[6] Iranzo A, Molinuevo JL, Santamaría J, Serradell M, Martí MJ, Valldeoriola F, et al. Rapid-eye-movement sleep behaviour disorder as an early marker for neurodegenerative disorder: a descriptive study. Lancet Neurol 2006;5:572–7.
[7] Iranzo A, Tolosa E, Gelpi E, Molinuevo JL, Valldeoriola F, Serradell M, et al. Neurodegenerative disease status and post-mortem pathology in idiopathic rapid-eye-movement sleep behaviour disorder: an observational cohort study. Lancet Neurol 2013;12:443–53.
[8] Peever J, Luppi PH, Montplaisir J. Breakdown in REM sleep circuitry underlies REM sleep behavior disorder. Trends Neurosci 2014;37:279–88.
[9] Lu J, Sherman D, Devor M, Saper CB. A putative flip-flop switch for control of REM sleep. Nature 2006;441:589–94.
[10] Datta S, MacLean RR. Neurobiological mechanisms for the regulation of mammalian sleep–wake behavior: reinterpretation of historical evidence and inclusion of contemporary cellular and molecular evidence. Neurosci Biobehav Rev 2007;31:775–824.
[11] Takakusaki K, Habaguchi T, Saitoh K, Kohyama J. Changes in the excitability of hindlimb motoneurons during muscular atonia induced by stimulating the pedunculopontine tegmental nucleus in cats. Neuroscience 2004;124:467–80.

[12] Saponjic J, Radulovacki M, Carley DW. Respiratory pattern modulation by the pedunculopontine tegmental nucleus. Respir Physiol Neurobiol 2003;138:223–37.
[13] Saponjic J, Cvorovic J, Radulovacki M, Carley DW. Serotonin and noradrenaline modulate respiratory pattern disturbance evoked by glutamate injection into the pedunculopontine tegmentum of anesthetized rats. Sleep 2005;28:560–70.
[14] Saponjic J, Radulovacki M, Carley DW. Injection of glutamate into the pedunculopontine tegmental nuclei of anesthetized rat causes respiratory dysrhythmia and alters EEG and EMG power. Sleep Breath 2005;9:82–91.
[15] Saponjic J, Radulovacki M, Carley DW. Modulation of respiratory pattern and upper airway muscle activity by the pedunculopontine tegmentum: role of NMDA receptors. Sleep Breath 2006;10:195–202.
[16] Rye DB. Contributions of the pedunculopontine region to normal and altered REM sleep. Sleep 1997;20:757–88.
[17] Semba K. Aminergic and cholinergic afferents to REM sleep induction regions of the pontine reticular formation in the rat. J Comp Neurol 1993;330:543–56.
[18] Losier BJ, Semba K. Dual projections of single cholinergic and aminergic brainstem neurons to the thalamus and basal forebrain in the rat. Brain Res 1993;604:41–52.
[19] Dringenberg HC, Olmstead MC. Integrated contributions of basal forebrain and thalamus to neocortical activation elicited by pedunculopontine tegmental stimulation in urethane-anesthetized rats. Neuroscience 2003;119:839–53.
[20] Sarter M, Bruno JP. Cortical cholinergic inputs mediating arousal, attentional processing and dreaming: differential afferent regulation of the basal forebrain by telencephalic and brainstem afferents. Neuroscience 2000;95:933–52.
[21] Pienaar IS, Harrison IF, Elson JL, Bury A, Woll P, Simon AK, et al. An animal model mimicking pedunculopontine nucleus cholinergic degeneration in Parkinson's disease. Brain Struct Funct 2014, http://dx.doi.org/10.1007/s00429-013-0669-5.
[22] Kotagal V, Albin RL, Müller MLTM, Koeppe RA, Chervin RD, Frey KA, et al. Symptoms of rapid eye movement sleep behavior disorder are associated with cholinergic denervation in Parkinson disease. Ann Neurol 2012;71:560–8.
[23] Kotagal V, Müller MLTM, Kaufer DI, Koeppe RA, Bohnen NI. Thalamic cholinergic innervation is spared in Alzheimer disease compared to Parkinsonian disorders. Neurosci Lett 2012;514:169–72.
[24] Bohnen NI, Albin RL. The cholinergic system and Parkinson disease. Behav Brain Res 2011;221:564–73.
[25] Bohnen NI, Müller MLTM, Koeppe RA, Studenski SA, Kilbourn MA, Fey KA, et al. History of falls in Parkinson disease is associated with reduced cholinergic activity. Neurology 2009;73:1670–6.
[26] Bezard E, Przedborski S. A tale on animal model of Parkinson's disease. Mov Disord 2011;26:993–1002.
[27] Balandini F, Armentero MT, Martignoni E. The 6-hydroxydopamine model: news from the past. Parkinsonism Relat Disord 2008;14(Suppl. 2):S124–9.
[28] Baladini F, Armentero MT. Animal models of Parkinson's disease. FEBS J 2012;279:1156–66.
[29] Duty S, Jenner P. Animal models of Parkinson's disease: a source of novel treatments and clues to the cause of the disease. Br J Pharmacol 2011;164:1357–91.
[30] Pineaar IS, van de Berg W. A non-cholinergic neuronal loss in the pedunculopontine nucleus of toxin-evoked parkinsonian rats. Exp Neurol 2013;248:213–23.
[31] Petrovic J, Lazic K, Ciric J, Kalauzi A, Saponjic J. Topography of the sleep/wake states related EEG microstructure and transitions structure differentiates the functionally distinct cholinergic innervation disorders in rat. Behav Brain Res 2013;256:108–18.
[32] Saponjic J, Petrovic J, Kalauzi A, Ciric J, Lazic K, Radulovacki M, et al. Sleep-state related EEG amplitude distribution in the rat model of cortical cholinergic innervation disorder. Sleep Biol Rhythm 2013;11:105–15.
[33] Petrovic J, Ciric J, Lazic K, Kalauzi A, Saponjic J. Lesion of the pedunculopontine tegmental nucleus in rat augments cortical activation and disturbs sleep/wake state transitions structure. Exp Neurol 2013;247:562–71.
[34] Saponjic J, Radulovacki M, Carley DW. Monoaminergic system lesions increase post-sigh respiratory pattern disturbance during sleep in rats. Physiol Behav 2007;90:1–10.
[35] Paxinos G, Watson C. The rat brain in stereotaxic coordinates. 5th ed. San Diego, USA: Elsevier Academic Press; 2005.
[36] Inglis WL, Semba K. Discriminable excitotoxic effects of ibotenic acid, AMPA, NMDA and quinolinic acid in the rat laterodorsal tegmental nucleus. Brain Res 1997;755:17–27.
[37] Paxinos G, Watson C, Carrive P, Kirkcaldie M, Ashwell KWS. Chemoarchitectonic atlas of the rat brain. 2nd ed. London, UK: Academic Press; 2009.
[38] Yan MM, Xu XH, Huang ZL, Yao MH, Urade Y, Qu WM. Selection of optimal epoch duration in assessment of rodent sleep–wake profiles. Sleep Biol Rhythm 2011;9:46–55.
[39] Jung KY, Cho JH, Ko D, Seok HY, Yoon HK, Lee HJ, et al. Increased corticomuscular coherence in idiopathic REM sleep behavioral disorder. Front Neurol 2012;3:1–6.
[40] Ushiyama J, Takahashi Y, Ushiba J. Muscle dependency of corticomuscular coherence in upper and lower limb muscles and training-related alterations in ballet dancers and weightlifters. J Appl Physiol 2010;109:1086–95.
[41] Kamp D, Krause V, Butz M, Schnitzler A, Pollok B. Changes of cortico-muscular coherence: an early marker of healthy aging. Age 2013;35:49–58.
[42] Krause V, Wach C, Sudmeyer M, Ferrea S, Schnitzler A, Pollok B. Cortico-muscular coupling and motor performance are modulated by 20 Hz transcranial alternating current stimulation (tACS) in Parkinson's disease. Front Hum Neurosci 2014;7:1–10.
[43] Kristeva R, Patino L, Omlor W. Beta-range cortical motor spectral power and corticomuscular coherence as a mechanism for effective corticospinal interaction during steady-state motor output. NeuroImage 2007;36:785–92.
[44] Salenius S, Avikainen S, Kaakkola S, Hari R, Brown P. Defective cortical drive to muscle in Parkinson's disease and its improvement with levodopa. Brain 2002;125:491–500.
[45] Moroni F, Nobili L, De Carli F, Massimini M, Francione S, Marzano C, et al. Slow EEG rhythms and inter-hemispheric synchronization across sleep and wakefulness in the human hippocampus. NeuroImage 2012;60:497–504.
[46] Genzel L, Dresler M. Sleep-more local and complex than previously thought. Front Neurol 2012;3:1–2.
[47] Braak H, Del Tredici K, Rüb U, de Vos RA, Jansen Steur EN, Braak E. Staging of brain pathology related to sporadic Parkinson's disease. Neurobiol Aging 2003;24:197–211.
[48] Engel AK, Fries P. Beta-band oscillations – signaling the status quo. Curr Opin Neurobiol 2010;20:156–65.
[49] Grace KP, Hughes SW, Horner RL. Identification of the mechanism mediating genioglosus muscle suppression in REM sleep. Am J Respir Crit Care Med 2013;187:311–9.
[50] Torontali ZA, Grace KP, Horner R, Peever JH. Cholinergic involvement in control of REM sleep paralysis. J Physiol 2014;592:1425–6.
[51] Jenkinson N, Nandi D, Muthusamy K, Ray NJ, Gregory R, Stein JF, et al. Anatomy, physiology, and pathophysiology of the pedunculopontine nucleus. Mov Disord 2009;24:319–28.
[52] Alam M, Schwabe K, Krauss JK. The pedunculopontine nucleus area: critical evaluation of interspecies differences relevant for its use as a target for deep brain stimulation. Brain 2011;134:11–23.
[53] Futami T, Takakusaki K, Kitai ST. Glutamatergic and cholinergic inputs from the pedunculopontine tegmental nucleus to dopamine neurons in the substantia nigra pars compacta. Neurosci Res 1995;21:331–42.
[54] Hur EE, Zaborszky L. Vglut2 afferents to the medial prefrontal and primary somatosensory cortices: a combined retrograde tracing in situ hybridization study. J Comp Neurol 2005;483:351–73.
[55] Kaur S, Junek A, Black MA, Semba K. Effects of ibotenate and 192IgG-saporin lesions of the nucleus basalis magnocellularis/substantia innominata on spontaneous sleep and wake states and on recovery sleep after sleep deprivation in rats. J Neurosci 2008;28:491–504.
[56] Lavoie B, Parent A. Pedunculopontine nucleus in the squirrel monkey: distribution of cholinergic and monoaminergic neurons in the mesopontine tegmentum with evidence for the presence of glutamate in cholinergic neurons. J Comp Neurol 1994;344:190–209.
[57] Rugg EL, Dunbar JS, Latimer M, Winn P. Excitotoxic lesions of the pedunculopontine tegmental nucleus of the rat I. Comparison of the effects of various excitotoxins, with particular reference to the loss of immunohistochemically identified cholinergic neurons. Brain Res 1992;589:181–93.